
Article:
Bernert, M., Janky, F., Sieglin, B. et al. (16 more authors) (2021) X-point radiation, its control and an ELM suppressed radiating regime at the ASDEX Upgrade tokamak. Nuclear Fusion. 024001. ISSN 1741-4326

https://doi.org/10.1088/1741-4326/abc936

---

1. Introduction to the X-point radiation regime

Detached divertor operation is required for future fusion devices in order to reduce the heat loads and meet the material limit of the divertor target plates [1]. In tokamaks with metal walls, like JET or ASDEX Upgrade (AUG), this is achieved in H-mode by seeding of extrinsic impurities, such as nitrogen or argon [2]. With the achievement of pronounced detachment [3], it is observed that the divertor radiation is concentrated in a small region in the vicinity of the X-point [4, 2]. The vertical extent of this region (FWHM) is about 5 cm for AUG. Usually the total radiated power fraction ($f_{rad} = P_{rad,tot}/P_{heat}$) is above 75 % for these conditions. Figure 1 gives an example of the radiated power distribution for AUG, where the so-called X-point radiator (XPR) is present.

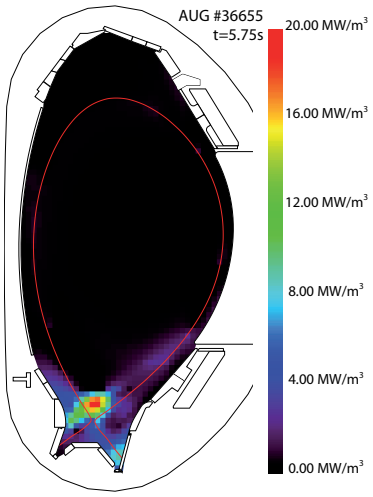

Figure 1. Tomographic reconstruction of the radiated power for AUG #36655, the X-point radiator is present.

Such behaviour was already observed at other machines [5, 6] and has similarities to the MARFE phenomenon [7]. It is assumed that the radiation is toroidally symmetric. The existence of such an intense power sink (the radiated power of this region can be above 5 MW in AUG) inside the confined plasma can be interpreted as a poloidally limited plasma, while at the midplane residual power and particle fluxes into the SOL still seem to exist. Plasmas operated in the X-point radiating regime stay in H-mode and do not necessarily develop into disruptions, which makes it a viable scenario for future reactors. Such X-point radiation is observed in all H-mode discharges in which the outer divertor detaches due to nitrogen seeding, for a wide range of auxiliary heating power 2.5 MW $\leq P_{heat} \leq$ 20 MW ($1 \leq \frac{P_{heat}}{P_{LH}} \leq 5$, P_{LH} being the power threshold for access to H-mode, here calculated based on the scaling in [8]). Similar observations can also be made with argon seeding, however, this is not yet broadly studied. With neon or krypton seeding no stable exhaust-relevant scenario has yet been achieved at AUG [2].

The location of the radiation relative to the X-point depends on the degree of detachment [9], which is decreasing with heating power and increasing with the seeding level. The X-point radiator is observed up to 15 cm above the X-point inside the confined region of the plasma, corresponding to a normalized poloidal flux of $\rho_{pol} \approx 0.985$ due to the large flux expansion in the X-point region. An intentional movement of the radiator is shown in Fig. 2, where either the heating power or the seeding level was varied to influence the XPR position. The AXUV diode bolometer diagnostic [10] is used to locate the XPR. The measured profile of a horizontally viewing camera (DLX) is shown over time in the middle plot, clearly showing the movement of the radiation peak. In the bottom row the measurements of all AXUV lines of sight (LOS) observing the divertor are shown for three time points, the detected location of the radiator is highlighted in red.

Measurements of deuterium line radiation below the XPR as well as SOLPS modelling [4] indicate that the plasma cools down to a few eV in the region between the XPR and the X-point, leading to poloidal temperature gradients inside the confined region.

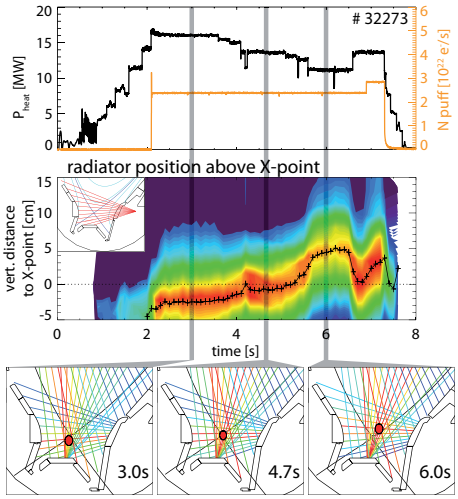

Figure 2. Position of the radiator for AUG discharge #32273. Top: Heating power and N seeding level; Middle: Contour plot of DLX measurements (geometry shown in the inlay) relative to the X-point height and detected position of the radiator (black); Bottom: LOS geometry and measurements for 3 time points, the relative intensity of each camera is color coded.

Similar to MARFEs, the development of the X-point radiation can be explained by a radiation condensation [11]. However, with nitrogen or argon as the dominant radiation species, this takes place at higher electron temperatures than with deuterium in unseeded discharges and recombination processes are, thus, not necessarily activated inside the confined region. This could also explain why a radiation condensation initialized by a high impurity content does not lead to an immediate disruption.

2. Real time control of the radiator position

For the real time control of the radiator, an automated detection mechanism for the vertical position of the radiator relative to the X-point was developed. The algorithm uses the measurements of the DLX camera (see inlay Fig. 2). The real-time data acquisition is based on the SIO2 system [12], the minimum cycle time is 1 ms with a time resolution of 5 µs.

As only the inter-ELM values are required, the ELM signals are filtered out by a real time percentile calculation similar to a median filter. A filter width of about 20 ms is necessary to reliably remove ELM signals. For the real-time detection, only channels 2–11 of 16 of the DLX camera are used. This allows us to localize the radiator from about 10 cm below to 20 cm above the usual X-point position.

The peak in radiation observed by the DLX camera defines the location of the X-point radiator. Example camera measurements are presented in Fig. 3, showing the pronounced radiation peak. In post processing, the peak of the measured (ELM-filtered) profile is fitted with a Gaussian curve, identifying the location, width and height of the peak.

For the real time application, a deterministic algorithm is required, therefore a simplified method instead of the iterative curve fitting is applied: For each time step, a linear offset, defined by channels 2 and 11 (green dashed line in Fig. 3), is removed from the measured profile; the first moment of the profile defines the location of the radiator.

The location of the magnetic X-point is taken from a real-time calculated magnetic equilibrium [13]. The detected height of the XPR, as defined by the DLX camera, is then mapped onto a vertical line through the X-point. This defines the vertical distance to the X-point, which is then used as control

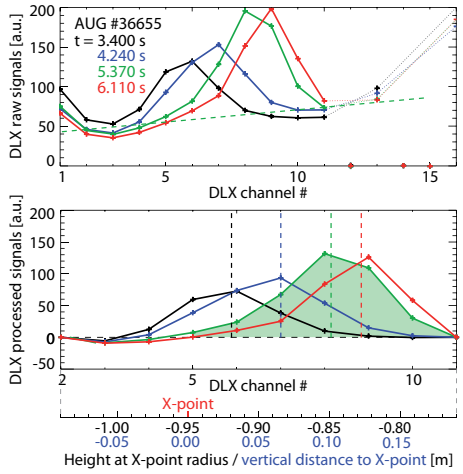

Figure 3. Detection principle of the X-point radiator for four time points in AUG #36655. Top: Median-filtered measurements of the DLX camera. A linear offset is subtracted (green dashed line). Bottom: Channels 2-11 are selected and the first moment is built, defining the position of the peak (dashed lines), and mapped to the vertical distance to the X-point.

parameter. The simplified peak detection by the first moment agrees with the peak location of a Gaussian curve fit within a few millimeters.

In comparison to other recently developed radiation control schemes for the X-point region [14] or divertor region [15], this controller is independent of the absolute radiation level and does not require a fixed target value, but takes advantage of the strong localization of the XPR and can adjust e.g. to different heating powers.

A PI controller is used to regulate the impurity seeding level depending on the mismatch of the measured and requested location of the XPR. This development benefited from previous work on the so-called Tdiv controller [16]. The gains of the new controller were adapted from the existing controller and optimised using a setup shot with pre-programmed seeding levels. Using the heating power as actuator is not implemented yet but planned for future use.

A series of discharges was conducted to demonstrate and optimise the controller, including variations of the request value, the heating power and the magnetic X-point position, see Figures 4–5. These discharges have a pre-programmed value for the nitrogen seeding up to 3 s, which is used to induce detachment and initiate the XPR. The detachment is identified by the reduction of the electron temperature and ion saturation currents measured by the Langmuir probes in the outer divertor (see first time point in Fig. 6 f & g). Thereafter, the target parameters change only marginally. This pre-seeding avoids erroneous detection of radiation peaks before an XPR exists. From 3 s on, the requested value for the location (shown in red) is changed as well as the auxiliary heating power, which is one of the main parameters to change the XPR location.

Figure 4 shows one of the first applications of the controller. The scatter of the detected XPR height is within 5 mm and the set value typically achieved within 1 cm. The discharge includes an upward shift of the requested location as well as a down stepping of the heating power. For a location higher than 3 cm, the controller becomes unstable and starts oscillating. Similar oscillations above 0 cm can be observed for the lower heating powers. Such oscillations could occur for a bifurcation between to detachment states of the plasma, similar to the so-called cliff-edge of detachment [17]. In [15], similar oscillations were observed and shown to arise from an instability of the plasma itself, most likely in correlation with the ELM activity. A real-time controller can drive and enhance such oscillations, if the inherent time delay of the controller is in the order of the oscillation period. The observed oscillation period of around $150 - 250$ ms is in the range of the

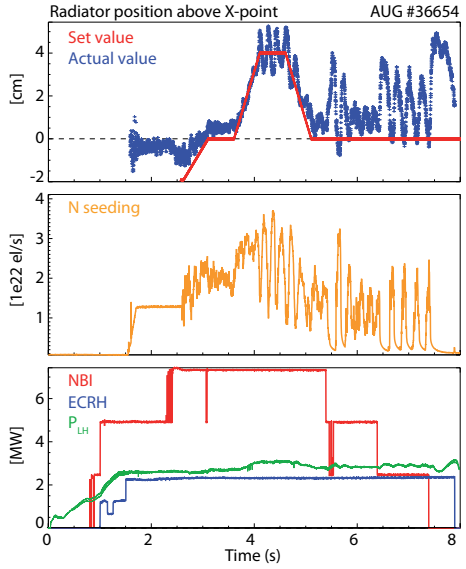

Figure 4. Overview of the XPR control for discharge #35554, control active from 3 s on: top: Set value and real time detected position of XPR; middle: Adjusted N seeding level; bottom: Heating power and L-H power threshold scaling [8].

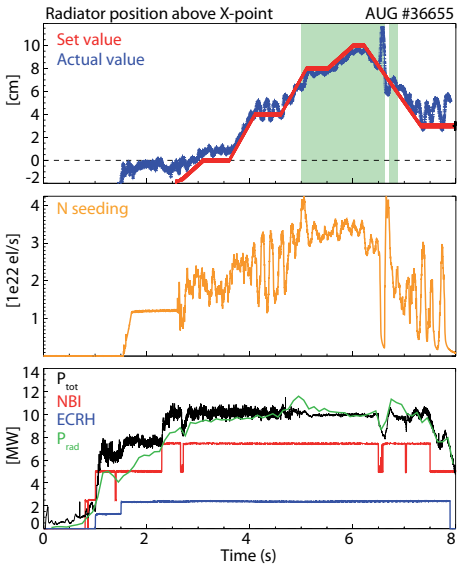

Figure 5. Overview of the XPR control for discharge #36655, same graphs as in Fig. 4, in addition the bottom graph shows the total heating power and the total radiated power. A phase during which ELMs are suppressed is highlighted in green, see Sec.3.

reaction time needed for the nitrogen seeding to influence the divertor plasma, which is usually around 50 ms (see [16]). With an optimized controller, it might be possible to damp such oscillations, however, they might not be fully avoided.

Note, that for the last heating step ($t \geq 7.4$ s in Fig. 4) the net heating power is nominally below the L-H power threshold scaling, even without the subtraction of radiation losses. In this phase plasma is still in H-mode, as ELMs can be observed, and the XPR is present, stable, and appears to be controllable, but on a slower time scale.

Figure 5 shows that the XPR can be controlled up to 10 cm inside the confined region. The strong oscillation of the controller seems to be only present for locations around $3-5$ cm. The long heating beam trip at 6.5 s shows that the radiator can penetrate further into the plasma and can still be controlled. However, due to the lack of experimental time, this has not yet been further investigated. The bottom of figure 5 also demonstrates that the radiated power fraction $f_{rad} = \frac{P_{rad}}{P_{tot}}$ does not change significantly but stays close to 100% while the XPR moves by several centimeters. This shows that the presented method allows a much finer control than systems based on the radiated power fraction.

In the discharge shown in Fig. 5, it is observed that ELM signatures disappear when the XPR is more than 7 cm inside the confined region. This regime of full detachment, quite high confinement, and no ELMs is further discussed in the following section.

3. An ELM-suppressed scenario for radiator locations far inside the confined region

With a location of the XPR high inside the confined region, in the case of Fig. 5 about 7 cm above the X-point, it is observed that typical ELM signatures, such as peaks in SOL currents or divertor radiation or a quasi-periodical reduction of stored energy, disappear. Figure 6 gives an overview of different time traces and profile measurements before and during the ELM-suppressed phase, which is highlighted in green. The transition is characterized by a reduction of the plasma density of about 15 % (Fig. 6b) while the stored energy is reduced by about 10 % (Fig. 6a). This leads to a marginal reduction of the H-factor to $H_{98} \approx 0.95$ (Fig. 6c). During this phase, the outer divertor is fully detached (Fig. 6 f & g) and the intermittent peaks or transient reattachment due to ELMs disappear. Even though the particle flux to the divertor target is significantly reduced, the neutral compression of the divertor slightly increases. The core tungsten concentration reduces from $4 \cdot 10^{-5}$ to $2.5 \cdot 10^{-5}$. The core nitrogen concentration in this phase is around 2–2.3 %. The trip of heating power and following counteractive measure by the XPR controller at 6.5 s leads to an oscillation of the XPR location around 7 cm, showing that ELM signatures reappear below 7 cm, but are then suppressed again as soon as the radiator is above that value.

During the ELM-suppressed phase, a weak pedestal is present at the plasma edge (Fig. 6d & e). The minimum $E \times B$ velocity in the pedestal is -6 km/s (measured by CXRS, [18]) and close to the threshold for H-mode of about -7 km/s [19]. The radial velocity of SOL filaments is estimated to be 560 m/s. These values are in between the typical values for L- and H-mode, quoted as 330 m/s and 1400 m/s, respectively [20]. As such, it cannot clearly be decided whether this phase is an H- or L-mode.

Similar observations of short phases of ELM-suppression at a high location of the XPR are made in discharges with feed forward programmed nitrogen seeding (e.g. AUG #36276 [4]). Without the active control of the XPR location, the ELM-suppressed phases were not sustained. The application of the XPR controller allows a stable operation in this regime. The ELM suppressed regime can reliably be recovered by controlling the XPR position on a high location. This regime was so far observed at auxiliary heating powers of $2.5 - 10$ MW, but the full operational range in heating power and plasma density is not yet explored.

In comparison to previously reported highly radiative regimes with high confinement (e.g. the RI mode) [21], the confinement does not additionally improve but decreases slightly from the high confinement of the H-mode. The decrease in density indicates that pedestal transport is changing and not only a radiative cooling takes place. The latter would be expressed in an increase of density.

4. Summary

A strong localisation of the radiation in the vicinity of the X-point is observed in nitrogen induced detachment in H-modes at ASDEX Upgrade. This so-called X-point radiator (XPR), which is similar to a MARFE, is observed to move inside the confined region. It exists for a wide range of heating power ($2 - 25$ MW) and is correlated with radiated power fractions of more than 75 %. There are indications of electron temperatures in the range of a few eV in the region of the XPR and below, leading to parallel electron temperature gradients inside the confined region. The XPR can stably exist up to 15 cm inside the confined region, corresponding to a normalized

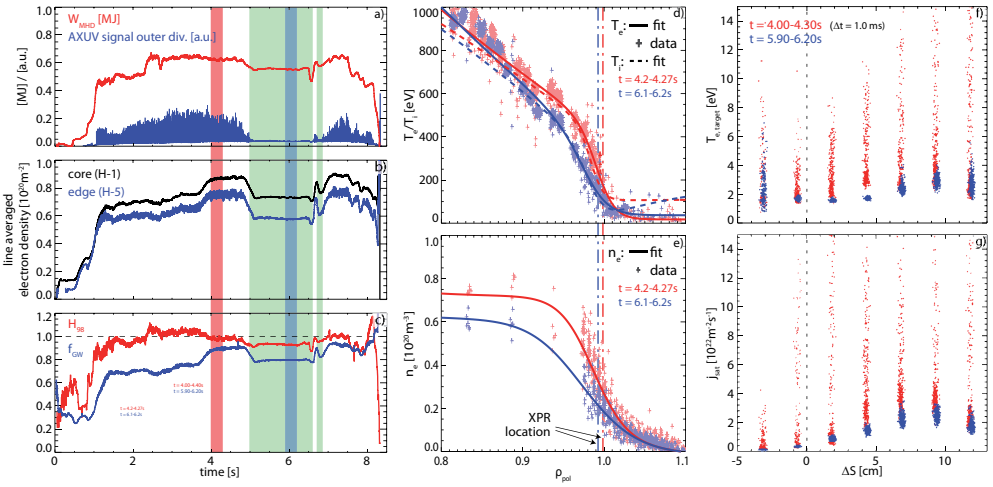

Figure 6. Measurements of discharge AUG #36655, where the X-point radiator control is active and an ELM-suppressed regime is observed (highlighted in green as in Fig. 5). Time traces of (a) plasma stored energy and an ELM indicator (AXUV LOS in the outer divertor), (b) line averaged density and (c) energy confinement time with respect to the ITERH98P(y,2) scaling and Greenwald density fraction. The red and blue shaded regions indicate the time windows for the profile measurements in (d-g). Pedestal profiles of (d) electron and ion temperature and (e) electron density, indicating also the radial location of the XPR. Langmuir probe measurements of (f) electron temperature and (g) ion saturation current at the outer divertor target, relative to the strikeline position.

radius of $\rho_{pol} \approx 0.985$, but is usually observed closer to the X-point, between $\rho_{pol} = 0.99$ and 1. The location is shown to be dependent on the nitrogen seeding level and heating power and thus can be actively controlled.

A real-time control scheme for the location of the XPR is implemented, using AXUV diodes as sensors and the nitrogen seeding level as actuator. The controller is shown to handle the location close to the X-point for a wide range of heating powers. The location can be controlled up to 10 cm inside the confined region. Some oscillations at low heating powers or at certain locations indicate that the controller might be marginally stable and needs further optimisation.

Applying this XPR control in experiment, a regime with ELM suppression was observed for a high location of the XPR. In this phase, the confinement is marginally reduced to $H_{98} \approx 0.95$. The values for the radial electric field well or the radial filament velocity lie between the typical values for L- or H-mode. Nonetheless, the relatively high confinement, high core electron and ion temperatures, the suppression of ELMs and full detachment at a radiated power fraction of up to 100 % makes this a promising candidate for a scenario of a future fusion reactor.

5. Outlook and future work

To understand the dominant physical mechanisms of the X-point radiator and its effect on the pedestal, localized electron density and temperature measurements using the newly installed diver-

tor Thomson scattering system as well as spectroscopic methods will be used. This will allow the detailed reconstruction of the heat flux involving such a localized highly radiating zone within the confined region.

The controller of the XPR position will be further optimized by a better tuning of the control parameters, also dynamically adjusting to other input parameters, such as the heating power. Thus, the controller will work stably in a wider operational range. Further developments may include the extension to other seeding gases and coupling to other existing controllers, such as the Tdiv controller [16], or the integration into schemes for disruption avoidance (e.g. at the H-mode density limit [22]).

Because the XPR has also been observed in seeded scenarios at JET [2, 23], and as the detached, seeded regime is a foreseen scenario in ITER, the control of the XPR might provide for future machines a robust method to stay in a regime with detached divertor, without large ELMs and contribute to the avoidance of disruptions in future machines.

Acknowledgement

This work has been carried out within the framework of the EUROfusion Consortium and has received funding from the Euratom research and training programme 2014-2018 and 2019-2020 under grant agreement No 633053. The views and opinions expressed herein do not necessarily reflect those of the European Commission.

References

[1] R.A. Pitts, X. Bonnin, F. Escourbiac, H. Frerichs, J.P. Gunn, T. Hirai, A.S. Kukushkin, E. Kaveeva, M.A. Miller, D. Moulton, V. Rozhansky, I. Senichenkov, E. Sytova, O. Schmitz, P.C. Stangeby, G. De Temmerman, I. Veselova, and S. Wiesen. Physics basis for the first ITER tungsten divertor. *Nuclear Materials and Energy*, 20:100696, 2019.

[2] M. Bernert, M. Wischmeier, A. Huber, F. Reimold, B. Lipschultz, C. Lowry, S. Brezinsek, R. Dux, T. Eich, A. Kallenbach, A. Lebschy, C. Maggi, R. McDermott, T. Pütterich, and S. Wiesen. Power exhaust by SOL and pedestal radiation at ASDEX Upgrade and JET. *Nuclear Materials and Energy*, 12:111 – 118, 2017. Proceedings of the 22nd International Conference on Plasma Surface Interactions 2016, 22nd PSI.

[3] A. Kallenbach, M. Bernert, M. Beurskens, L. Casali, M. Dunne, T. Eich, L. Giannone, A. Herrmann, M. Maraschek, S. Potzel, F. Reimold, V. Rohde, J. Schweinzer, E. Viezzer, M. Wischmeier, and the ASDEX Upgrade Team. Partial detachment of high power discharges in ASDEX Upgrade. *Nuclear Fusion*, 55(5):053026, 2015.

[4] F. Reimold, M. Wischmeier, M. Bernert, S. Potzel, A. Kallenbach, H.W. Müller, B. Sieglin, U. Stroth, and the ASDEX Upgrade Team. Divertor studies in nitrogen induced completely detached H-modes in full tungsten ASDEX Upgrade. *Nuclear Fusion*, 55(3):033004, 2015.

[5] T. Nakano, H. Kubo, N. Asakura, K. Shimizu, H. Kawashima, and S. Higashijima. Radiation process of carbon ions in JT-60U detached divertor plasmas. *Journal of Nuclear Materials*, 390-391:255 – 258, 2009. Proceedings of the 18th International Conference on Plasma-Surface Interactions in Controlled Fusion DeviceProceedings of the 18th International Conference on Plasma-Surface Interactions in Controlled Fusion Device.

[6] J. A. Goetz, B. LaBombard, B. Lipschultz, C. S. Pitcher, J. L. Terry, C. Boswell, S. Gangadhara, D. Pappas, J. Weaver, B. Welch, R. L. Boivin, P. Bonoli, C. Fiore, R. Granetz, M. Greenwald, A. Hubbard, I. Hutchinson, J. Irby, E. Marmar, D. Mossessian, M. Porkolab, J. Rice, W. L. Rowan, G. Schilling, J. Snipes, Y. Takase, S. Wolfe, and S. Wukitch. High confinement dissipative divertor operation on Alcator C-Mod. *Physics of Plasmas*, 6(5):1899–1906, 1999.

[7] B. Lipschultz, B. LaBombard, E.S. Marmar, M.M. Pickrell, J.L. Terry, R. Watterson, and S.M. Wolfe. MARFE: an edge plasma phenomenon. *Nuclear Fusion*, 24(8):977, 1984.

[8] Y R Martin, T Takizuka, and the ITPA CDBM H-mode Threshold Database Working Group. Power requirement for accessing the H-mode in ITER. *Journal of Physics: Conference Series*, 123(1):012033, 2008.

[9] A Loarte, R.D Monk, J.R Martín-Solís, D.J Campbell, A.V Chankin, S Clement, S.J Davies, J Ehrenberg, S.K Erents, H.Y Guo, P.J Harbour, L.D Horton, L.C Ingesson, H Jäckel, J Lingertat, C.G Lowry, C.F Maggi, G.F Matthews, K McCormick, D.P O'Brien, R Reichle, G Saibene, R.J Smith, M.F Stamp, D Stork, and G.C Vlases. Plasma detachment in JET mark i divertor experiments. *Nuclear Fusion*, 38(3):331–371, mar 1998.

[10] M. Bernert, T. Eich, A. Burckhart, J. C. Fuchs, L. Giannone, A. Kallenbach, R. M. McDermott, B. Sieglin, and ASDEX Upgrade Team. Application of AXUV diode detectors at ASDEX Upgrade. *Review of Scientific Instruments*, 85(3), 2014.

[11] J. F. Drake. Marfes: Radiative condensation in tokamak edge plasma. *The Physics of Fluids*, 30(8):2429–2433, 1987.

[12] K. Behler, H. Blank, H. Eixenberger, M. Fitzek, A. Lohs, K. Lüddecke, and R. Merkel. Deployment and future prospects of high performance diagnostics featuring serial I/O (SIO) data acquisition (DAQ) at ASDEX Upgrade. *Fusion Engineering and Design*, 87(12):2145 – 2151, 2012. Proceedings of the 8th IAEA Technical Meeting on Control, Data Acquisition, and Remote Participation for Fusion Research.

[13] L. Giannone, M. Reich, M. Maraschek, E. Poli, C. Rapson, L. Barrera, R. McDermott, A. Mlynek, Q. Ruan, W. Treutterer, L. Wenzel, A. Bock, G. Conway, R. Fischer, J.C. Fuchs, K. Lackner, P.J. McCarthy, R. Preuss, M. Rampp, K.H. Schuhbeck, J. Stober, and H. Zohm. A data acquisition system for real-time magnetic equilibrium reconstruction on ASDEX Upgrade and its application to NTM stabilization experiments. *Fusion Engineering and Design*, 88(12):3299 – 3311, 2013.

[14] G.S. Xu, Q.P. Yuan, K.D. Li, L. Wang, J.C. Xu, Q.Q. Yang, Y.M. Duan, L.Y. Meng, Z.S. Yang, F. Ding, J.B. Liu, H.Y. Guo, H.Q. Wang, D. Eldon, Y.Q. Tao, K. Wu, N. Yan, R. Ding, Y.F. Wang, Y. Ye, L. Zhang, T. Zhang, Q. Zang, Y.Y. Li, H.Q. Liu, G.Z. Jia, X.J. Liu, H. Si, E.Z. Li, L. Zeng, J.P. Qian, S.Y. Lin, L.Q. Xu, H.H. Wang, X.Z. Gong, and B.N. Wan and. Divertor impurity seeding with a new feedback control scheme for maintaining good core confinement in grassy-ELM h-mode regime with tungsten monoblock divertor in EAST. *Nuclear Fusion*, 60(8):086001, jul 2020.

[15] D. Eldon, E. Kolemen, D.A. Humphreys, A.W. Hyatt, A.E. Järvinen, A.W. Leonard, A.G. McLean, A.L. Moser, T.W. Petrie, and M.L. Walker. Advances in radiated power control at DIII-D. *Nuclear Materials and Energy*, 18:285 – 290, 2019.

[16] A Kallenbach, R Dux, J C Fuchs, R Fischer, B Geiger, L Giannone, A Herrmann, T Lunt, V Mertens, R McDermott, R Neu, T Pütterich, S Rathgeber, V Rohde, K Schmid, J Schweinzer, W Treutterer, and ASDEX Upgrade Team. Divertor power load feedback with nitrogen seeding in ASDEX Upgrade. *Plasma Physics and Controlled Fusion*, 52(5):055002, 2010.

[17] A. E. Järvinen, S. L. Allen, D. Eldon, M. E. Fenstermacher, M. Groth, D. N. Hill, A. W. Leonard, A. G. McLean, G. D. Porter, T. D. Rognlien, C. M. Samuell, and H. Q. Wang. $E \times B$ flux driven detachment bifurcation in the DIII-D tokamak. *Phys. Rev. Lett.*, 121:075001, Aug 2018.

[18] M Cavedon, T Pütterich, E Viezzer, F M Laggner, A Burckhart, M Dunne, R Fischer, A Lebschy, F Mink, U Stroth, M Willensdorfer, and E Wolfrum and. Pedestal and E_r profile evolution during an edge localized mode cycle at ASDEX Upgrade. *Plasma Physics and Controlled Fusion*, 59(10):105007, aug 2017.

[19] M. Cavedon, G. Birkenmeier, T. Pütterich, F. Ryter, E. Viezzer, E. Wolfrum, R. Dux, T. Happel, P. Hennequin, U. Plank, U. Stroth, and M. Willensdorfer and. Connecting the global H-mode power threshold to the local radial electric field at ASDEX Upgrade. *Nuclear Fusion*, 60(6):066026, may 2020.

[20] M. Griener, E. Wolfrum, M. Cavedon, R. Dux, V. Rohde, M. Sochor, J. M. Munoz Burgos, O. Schmitz, and U. Stroth. Helium line ratio spectroscopy for high spatiotemporal resolution plasma edge profile measurements at ASDEX Upgrade (invited). *Review of Scientific Instruments*, 89(10):10D102, 2018.

[21] J Ongena, A M Messiaen, B Unterberg, R V Budny, C E Bush, K Hill, G T Hoang, G Jackson, A Kallenbach, P Monier-Garbet, D Mueller, M Murakami, G Staebler, F Ryter, M Wade, M Bell, J Boedo, G Bonheure, P Du-

mortier, F Durodie, K H Finken, G Fuchs, B Giesen, P Hütteman, R Jaspers, R Koch, A Krämer-Flecken, Ph Mertens, R Moyer, A Pospieszczyk, A Ramsey, U Samm, M Sauer, B Schweer, R Uhlemann, P E Vandenplas, G Van Oost, M Vervier, G Van Wassenhove, G Waidmann, R R Weynants, G H Wolf, , , and and. Overview of experiments with radiation cooling at high confinement and high density in limited and diverted discharges. *Plasma Physics and Controlled Fusion*, 41(3A):A379–A399, jan 1999.

[22] *Rapid prototyping of advanced control schemes in ASDEX Upgrade*, 2019. 12th IAEA Technical Meeting on Control, Data Acquisition and Remote Participation for Fusion Research (CODAC 2019).

[23] S. Glöggler, M. Wischmeier, E. Fable, E.R. Solano, M. Sertoli, M. Bernert, G. Calabrò, M. Chernyshova, A. Huber, E. Kowalska-Strzeciwilk, C. Lowry, E. de la Luna, C.F. Maggi, U. Stroth, H.J. Sun, M.L. Reinke, and S. Wiesen and. Characterisation of highly radiating neon seeded plasmas in JET-ILW. *Nuclear Fusion*, 59(12):126031, oct 2019.